frontiers | Frontiers in Physics

TYPE Original Research
PUBLISHED 15 August 2022
DOI 10.3389/fphy.2022.969921

OPEN ACCESS

EDITED BY
Zhiwen Liu,
The Pennsylvania State University (PSU), United States

REVIEWED BY
Bormashenko Edward,
Ariel University, Israel
Jinda Lin,
Shanghai Institute of Optics and Fine Mechanics, China

*CORRESPONDENCE
Anpei Ye,
yap@pku.edu.cn

SPECIALTY SECTION
This article was submitted to Atomic and Molecular Physics, a section of the journal Frontiers in Physics

RECEIVED 15 June 2022
ACCEPTED 11 July 2022
PUBLISHED 15 August 2022

CITATION
Tong Y-K, Meng X, Zhou B, Sun R, Wu Z, Hu M and Ye A (2022), Detecting the pH-dependent liquid-liquid phase separation of single levitated aerosol microdroplets via laser tweezers-Raman spectroscopy.
Front. Phys. 10:969921.
doi: 10.3389/fphy.2022.969921

Detecting the pH-dependent liquid-liquid phase separation of single levitated aerosol microdroplets *via* laser tweezers-Raman spectroscopy

Yu-Kai Tong[1], Xiangxinyue Meng[2], Bo Zhou[1,3], Rui Sun[1], Zhijun Wu[2], Min Hu[2] and Anpei Ye[1]*

[1]Key Laboratory for the Physics and Chemistry of Nanodevices, School of Electronics, Peking University, Beijing, China, [2]State Key Joint Laboratory of Environmental Simulation and Pollution Control, College of Environmental Sciences and Engineering, Peking University, Beijing, China, [3]School of Science, Beijing University of Posts and Telecommunications, Beijing, China

Ambient atmospheric aerosol particles comprised of various inorganic and organic substances ubiquitously undergo phase transition, such as efflorescence, amorphization, and especially liquid-liquid phase separation (LLPS). Resultant changes of physicochemical properties in aerosols then deeply affect the climate system. However, finely detecting these processes occurring in single aerosol particles, especially under the acidic condition of real atmospheric environment, remains a challenge. In this work, we investigated the pH-dependent phase separation in single levitated microdroplets using a self-developed laser tweezers Raman spectroscopy (LTRS) system. The dynamic process of LLPS in laser-trapped droplets over the course of humidity cycles was detected with the time-resolved cavity-enhanced Raman spectra. These measurements provide the first comprehensive account of the pH-dependent LLPS in single levitated aerosol microdroplets and bring possible implications on phase separation in actual atmospheric particles.

KEYWORDS

single aerosol, pH, liquid-liquid phase separation, Raman spectroscopy, laser tweezers

Introduction

Aerosol particles are prevalent in atmosphere and impact the climate system in two significant ways. One way is that aerosols directly influence solar radiation, e.g., aerosols containing sulfates and nitrates can scatter the solar radiation back into space and then reduce the temperature of atmosphere. The other way is that aerosols can act as cloud condensation nuclei, affect the number density of cloud droplets and indirectly impact the climate. These impacts on climate substantially depend on the critical physicochemical properties of aerosols, including optical properties [1,2], heterogeneous chemistry [3,4],

water uptake behavior [5,6], and nucleation activity [7–10]. These properties, in turn, are dictated by the morphology of the aerosols, especially the intern structure and phase state.

The liquid-liquid phase separation (LLPS), a distinctive morphology in aerosol microdroplets, has been investigated under various laboratory and out-field environments [9,11,12]. For laboratory works on LLPS in single aerosol droplets, Kwamena et al. [13] conducted experiments and simulation analysis on decane/NaCl/water droplets and found that the morphology of liquid-liquid phase separated droplets can be explicitly determined once given the values of surface/interface tension of the two phases. Reid et al. [14] investigated the LLPS in microdroplets with NaCl as the hydrophilic component and hydrocarbons, alcohols and fatty acids as the hydrophobic component. With the analysis of surface tension, they found that core-shell morphology predominates in the LLPS of aerosols whose organic components are water insoluble, while partially engulfed morphology predominates in the aerosols with water soluble organics. Stewart et al. [15] put forward three signatures of the time-solved cavity-enhanced Raman spectra to detect the LLPS in aqueous polyethylene glycol (PEG-400)/ammonium sulfate system and aqueous C6-diacids/ammonium sulfate system. Ishizaka et al. [16] used a temperature-responsive ionic liquid as a surrogate of the water insoluble organics and observed the partially engulfed morphology during the dehumidifying process of microdroplets.

For field studies, Pöhlker et al. [17] observed the atmospheric particles collected during the wet season in Amazonian rainforest through scanning electron microscopy, exhibited a LLPS structure with a salt core and an organic coating in the aerosols, and disentangled the impact of rainforests on the climate at the level of aerosols. You et al. [18] presented images that show the coexistence of two noncrystalline phases for real-world samples collected on multiple days in Atlanta. Lee et al. [19] produced primary sea spray aerosols from wave breaking of natural seawater within a wave flume and investigated the evolving heterogeneity within aerosol populations. They found that particles between ca. 0.3 and 1 μm in volume equivalent diameter displayed a LLPS morphology where an inorganic core was coated with an organic shell.

A caveat is that most of present studies focused merely on the influence of chemical composition on LLPS. However, even those works on real-world aerosols used the diluted extracts of filter-collected samples for aerosol generation where the constituent concentration differed from pristine atmosphere aerosols. Recent out-field studies have reported the high acidity found in many ambient aerosol particles [20–25]. Thus, it is imperative to detect the LLPS in microdroplets at their pristine state, that is, in acidic environment. Dallemagne et al. [26] found the variation in pH of aqueous PEG-400/$(NH_4)_2SO_4$ aerosols during LLPS where the pH in two liquid phases was of the same order of magnitude but with a difference of less than 0.4 pH units. Losey et al. [27,28] investigated the LLPS of microdroplets over the course of humidity cycles and found that the separation relative humidity (SRH, the RH level at which LLPS occurs) of organic acids increases as the droplet pH decreases, while the SRH of other organics (e.g., polyols) decreases as pH decreases.

TABLE 1 Information of the mother solutions used to generate aerosol droplets.

Solution ID	Solute	pH
OA-I	Oleic Acid + NaCl	7.07 ± 0.12*
OA-II		1.22 ± 0.08*
HEX-I		6.93 ± 0.11
HEX-II	1,2,6-hexanetriol	4.79 ± 0.08
HEX-III	+ $(NH_4)_2SO_4$	2.85 ± 0.12
HEX-IV		1.13 ± 0.07

*Data reported only for the aqueous compartment.

Such studies on the impact of pH on LLPS are limited. Nearly all used the substrate-deposited droplets as targets, where the influence of the contact coverslip on the morphology of the droplets cannot be excluded [29]. In this study, we investigated the pH-dependent LLPS of single laser-levitated microdroplets. First, we detected the LLPS in inherently separated droplets which were comprised of oleic acid (OA) and sodium chloride, and explored the possible change of LLPS morphology in acidic environment. Then, LLPS in internally miscible 1,2,6-hexanetriol/ammonium sulfate/water droplets with various pH were investigated during dehumidifying process. Finally, we analyzed and compared the influence of pH on phase separation in these aerosol droplets. To the best of the authors' knowledge, it is the first time to investigate the impact of pH on LLPS in single levitated aerosol droplets.

Method and experimental section

Reagents and single aerosol manipulation

Six mother solutions were used in this study to generate aerosol droplets which were grouped into two types, OA/NaCl and 1,2,6-hexanetriol (HEX)/$(NH_4)_2SO_4$. The solutions were prepared by double-distilled water (18.2 MΩ cm; Milli-Q; MilliporeSigma, Burlington, MA, United States). Taking account of that sulfates are one of the major inorganics in ambient aerosols, we adjusted the pH of the solutions by adding different amounts of sulfate acid (guaranteed reagent, Xilong Scientific Co., Ltd., Guangdong, China). Solute NaCl and $(NH_4)_2SO_4$ were purchased from Tong Guang Fine Chemical Co. (Beijing, China). Solute OA (analytical reagent) was purchased from Xilong Scientific Co., Ltd. (Guangdong, China); HEX was purchased from Shanghai Macklin

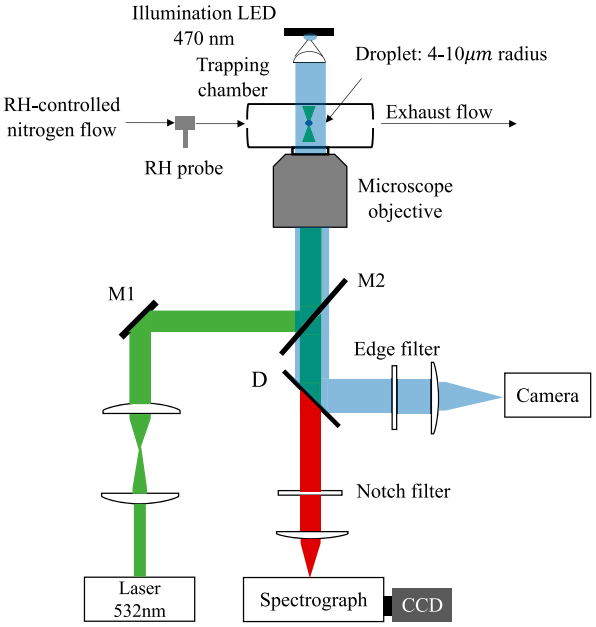

FIGURE 1
Schematic of the laser tweezers Raman spectroscopy (LTRS) system. A laser beam passes through a pair of beam expansion optics and finally couples into an objective to form the laser tweezers. The droplet is imaging using a 470 nm illumination LED and a high frame rate camera. The Raman spectra of the trapped droplets are recorded using a spectrograph/CCD. M1 and M2 are mirrors. D is a long pass dichroic mirror.

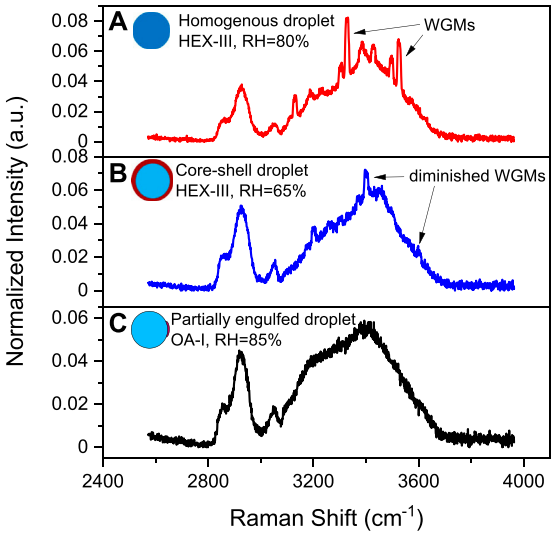

FIGURE 2
Raman spectra snapshots of microdroplets. **(A)** A Raman spectrum extracted from Figure 5A2 at 200 s, a homogenous droplet generated from HEX-III, RH = 80%. **(B)** A Raman spectrum extracted from Figure 5A2 at 1242 s, a core-shell droplet generated from HEX-III, RH = 65%. **(C)** A Raman spectrum extracted from Figure 3A at 613 s, a partially engulfed droplet generated from OA-I, RH=85%. The WGMs are pointed out with arrowed lines.

Biochemical Co.,Ltd. (Shanghai, China). Relevant information of the mother solutions is listed in Table 1. The pH of mother solutions was measured with a pH meter (Mettler Toledo Instruments Co., Ltd., Shanghai, China). All volume fractions of organics in the mother solutions used in this work were 10%. The organic-to-inorganic mass ratios (OIR) of Solution HEX-I ~IV are all 2/1.

A schematic of the laser tweezers Raman spectroscopy (LTRS) system is shown in Figure 1. Details of the single particle technique used here can be seen in our previous work [30,31]. In brief, we generated the aerosol droplets of desired chemical composition by a medical nebulizer (Mint PN100) and used a self-developed laser tweezers to trap a single levitated droplet (4 ~10 μm in radius). The droplet was trapped in a tailored chamber where the relative humidity (RH) could be regulated at a maximum rate of 5% RH/min by mixing dry and humidified nitrogen gas flow; the value of RH was monitored with a RH probe (HC2A-S, ROTRONIC). A laser beam with a wavelength of 532 nm (Excelsior-532-200, Spectra Physics) was used to both trap the aerosol droplet and excite its Raman signal, which was recorded by a spectrograph (SpectaPro 2300i, Acton) equipped with a liquid nitrogen cooled CCD (Spec-10, Princeton Instruments). We observed the LLPS of the single levitated droplet, which was generated from different mother solutions, during a dehumidifying process and determined the SRH according to the readouts of the RH probe.

The disturbance of the RH-controlled nitrogen flow was discussed in the Supplemental Material (Section S1) by calculating relevant dimensionless numbers including the Weber number and the Ohnesorge number. The results indicate that compared with the gravity, inertia and viscosity of the droplet, the surface tension is the dominant factor that impacts the morphology of the droplet. Thus, under the effect of self-surface tension, the single levitated droplet can be considered to be a stationary sphere after achieving a balance with the ambient atmosphere (see an image of the trapped droplet shown in Supplementary Figure S3 in the Supplemental Material).

Detection of liquid-liquid phase separation

The phase separation in substrate-deposited droplets has been directly observed by bright-field imaging or scanning electron microscopy [17–19,32]. However, for levitated droplets, the defocus of the trapped droplets blurs the direct imaging. Instead, the time-resolved Raman spectra of the trapped droplets can be used to detect the LLPS efficiently [13–15,33–36]. The Raman spectra demos from different kinds of microdroplets are shown in Figure 2. The trapped droplet works as an

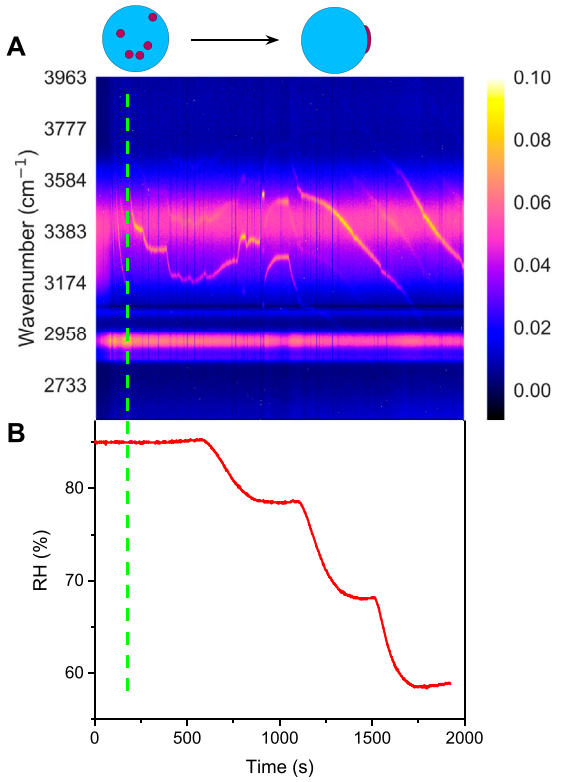

FIGURE 3
Liquid-liquid phase separation of aqueous oleic acid/sodium chloride (OA-I). **(A)** time-resolved Raman spectra and schematic diagram of phase separation, the bright trend dots indicate the position evolution of the detectable peaks (i.e., the WGMs shown in Figure 2). **(B)** RH variation with time in the trapping chamber during the dehumidifying process. The green dashed line indicates the moment when the random motion of inclusions in the droplet stopped and culminated in a stable partially-engulfed structure.

enhancing cavity and will overlap stimulated sharp peaks at wavelengths commensurate with whispering gallery modes (WGMs) on the spontaneous Raman spectra (see Figure 2A). The WGM peaks are extremely sensitive with the morphology of the droplet, indicating that if the droplet undergoes phase separation and becomes nonspherical (e.g., partially engulfed), WGM peaks in the spectra will quench (see Figure 2C). Thus, the moment when WGM peaks start to quench can be determined as the onset of phase separation, particularly for partially engulfed phase separation.

For the other mode of phase separation, the core-shell morphology, the sphericity of the phase separated droplet remains and its Raman spectra still retain WGM peaks (see Figure 2B). Nonetheless, the radial homogeneity is destroyed because of the separation of the hydrophilic core and hydrophobic shell. Thus, fitting the Raman spectra with the Mie scattering model for a homogenous droplet, the fitting errors between the measured and simulated WGM peaks are supposed to increase drastically (i.e. model failure). Therefore, the moment when the homogenous fitting errors start to soar can be determined as the onset of core-shell phase separation. The homogenous Mie scattering fitting model used in this work was developed by Preston et al. [37]. All the Raman spectra used here is normalized by area.

Results and discussion

In this work, we detected the phase separation of microdroplets comprised of various organics and inorganics at room temperature. In details, the aerosol droplets comprised of oleic acid/sodium chloride/water and 1,2,6-hexanetriol/ammonium sulfate/water were included, respectively. The pH of the droplets was adjusted by adding different amounts of sulfate acid. The phase separation of the internally miscible aerosol droplets under different acidic environment was realized by dehydrating the droplets.

Inherently separated aerosols

The number of organic species in a single atmospheric particle is on the order of thousands, among which water insoluble organic compounds (WIOCs) take a quite important part. Here, we used oleic acid as a surrogate of WIOC and detected the phase separation of inherently separated aerosols.

Figure 3A shows the time-resolved Raman spectra of the aerosol droplet generated from Solution OA-I, which vividly depicts the progression of phase separation. The brand range of 3100 ~3600 cm^{-1} corresponds to the bending and stretching modes of O-H of water, while the range of 2,850 ~ 2,950 cm^{-1} corresponds to the C-H mode of organics (OA here). In the beginning, the RH was set at a constant value of 85% for around 650 s to let the freshly trapped droplet reach a stable state. It can be seen that in the beginning (before ~230 s, marked with a green dashed line in Figure 3), there are no pronounced bright dots in the spectra which indicates that no WGMs have emerged in the freshly trapped droplet. It is because that the droplet was generated by nebulizing the mixture of OA/NaCl/Water and a number of emulsions of OA would certainly be contained in the nascent droplet. The random motion of the inclusions destroys the radial homogeneity and gives rise to the absence of the WGMs (see the schematic diagram in Figure 3A). After this, no more than one bright dot presents in each spectral snapshot which indicates that at most one WGM peak has been detected in the spectra of the droplet. It means that the droplet was heterogenous, in other words, phase-separation with a partially engulfed structure took place. The rather complex but very weak resonant structure in the spectra stems from that the volume of the aqueous inorganic phase may be far greater than that of the hydrophobic organic phase because of the

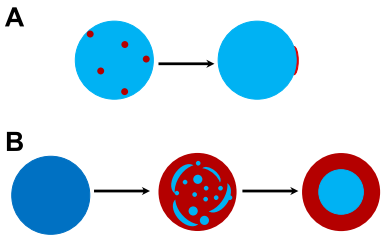

FIGURE 4
Schematic diagram of possible morphologies for the progression of phase separation. **(A)** phase separation of inherently separated aerosols, e.g., OA/NaCl/Water. **(B)** phase separation of internally miscible aerosols in a model of spinodal decomposition during dehumidifying, e.g., HEX/$(NH_4)_2SO_4$/Water. Dark blue: homogenous phase, light blue: hydrophilic phase, dark red: hydrophobic phase.

prior stochastic mixing of OA emulsions and water, and an approximately spherical cavity occurs for the aqueous volume (see the schematic diagram in Figure 4A). The imperfect spherical volume is supposed to lead to complexity in the WGM fingerprint and a low enhancement due to the low quality of the WGMs [14].

After adding sulfate acid, the phase separation of OA-II is shown in Supplementary Figure S1 (see the Supplemental Material). It can be seen that after the transient evolution of the nascent droplet, there are still several weak but non-eliminable WGM peaks in the spectral snapshots (100 ~400 s). It may be explained by that the added sulfate acid worked as a surfactant and reduced the surface tension between air and organic phase and the interface tension between organic and inorganic phase, which then changed the morphology of the phase separated droplet from partially engulfed structure to core-shell structure. However, such core-shell structure was quite fragile and lasted only for a short while. As the RH continued to decrease, the concentration of the inorganics as well as the surface tension between air and inorganic phase increased, which turned the core-shell structure back to partially engulfed structure. This change is shown in the spectral snapshots that as RH decreased, after ~430 s, the droplet was dehydrated and similar low-quality WGMs emerged. Besides, the interim process

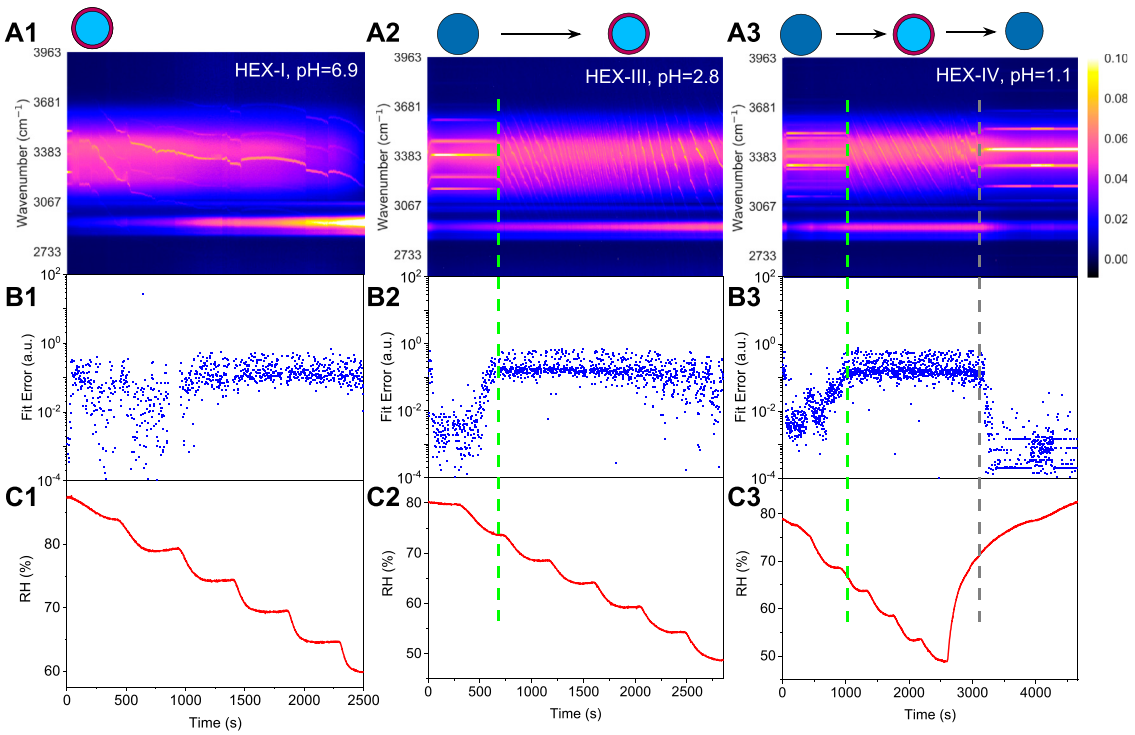

FIGURE 5
Liquid-liquid phase separation of 1,2,6-hexanetriol/ammonium sulfate/water. Top row: time-resolved Raman spectra and schematic diagrams of phase separation, the bright trend dots indicate the position evolution of the peaks. Middle row: fitting errors of the WGMs based on the homogenous Mie scattering model. Bottom row: RH variation with time in the trapping chamber during humidity steps. Panels **(A1–C1)**: aerosol generated from Solution HEX-I. Panels **(A2–C2)**: aerosol generated from Solution HEX-III, green dashed line indicates the moment when phase separation occurred. Panels **(A3–C3)**: aerosol generated from Solution HEX-IV, green dashed line and grey dashed line indicate the moment when phase separation and phase mixing occurred, respectively. Results of HEX-II (pH = 4.8) can be seen in Supplementary Figure S2 in the Supplemental Material.

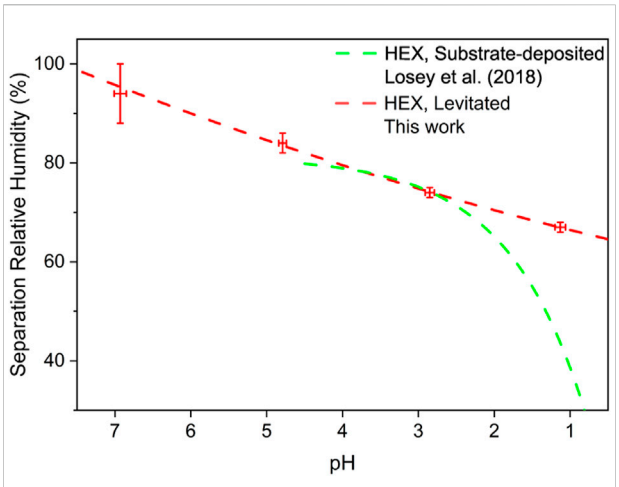

FIGURE 6
Separation relative humidity as a function of pH. Colors: red, droplets from Solution HEX-I ~IV, this work; green, droplets of 1,2,6-hexanetriol/ $(NH_4)_2SO_4$, [28]. The uncertainties in pH are the standard deviations resulting from averaging multiple measurements. The uncertainties in SRH mean the range where the exact values of SRH locate. The data points are the mediate values of the SRH ranges.

from partially-engulfed to core-shell is also illustrated in the time-resolved Raman spectra, where no WGMs were recorded during 400 ~430 s.

Internally miscible aerosols

The formation of ambient secondary organic aerosols (SOAs) is inextricable from the generation of organosulfates and nitrooxy-organosulfates [3,38,39], which then contributes to the emergence of various water soluble organic compounds (WSOCs). Most of the WSOCs are humic-like substances, including dicarboxylic acids, polyols, esters, and ethers. We used 1,2,6-hexanetriol as the surrogate of WSOC and detected the phase separation of internally miscible aerosols.

Figure 5 illustrates the phase separations of aerosol droplets generated from aqueous HEX/ $(NH_4)_2SO_4$ at different pH levels. For HEX-I (pH = 6.9), from Figure 5A1, we can see that there are numerous WGMs from the beginning of the time-resolved Raman spectra. After the droplet reaches a stable state with the ambient environment, there are still three WGMs in the spectral snapshots, one of which is quite prominent. It means that the droplet could not be partially-engulfed, in other words, the droplet was expected to be either core-shell or homogenous. In Figure 5B1, the fitting errors of the measured WGMs calculated by the homogenous Mie scattering model are on the order of 10^{-1} ~ 10^{0}, which are far greater than those from homogenous droplets (compared with Figure 5B2), time = 0–500 s). It also indicates that although the droplet was generated from a homogenous internally miscible solution, it underwent phase separation just after entering the optical well. Thus, the SRH of HEX-I is presumably higher than the initial RH (88%) in the trapping chamber.

For HEX-III (pH = 2.8), Figure 5A2) shows that before 690 s, the droplet was homogenous with five obvious WGMs in its spectra, and the fitting errors in Figure 5B2 are pretty minor. However, as the RH keeps decreasing, the fitting errors surge promptly (note the logarithmic scale), indicating that the phase state of the droplet changed during 690–700 s (marked with a dashed line in the figure). The corresponding RH shown in Figure 5C2 is in the range of 73%–75%, at which the SRH of HEX-III may locate. Previous works found that the mechanism of phase separation in aerosol microdroplet was mainly determined by the OIR of the droplet. Empirical summaries indicate that when 1/1.5 < OIR < 2, the LLPS occurs dominantly via spinodal decomposition [35]. Considering the OIR of HEX-III, the droplet may undergo phase separation by spinodal decomposition and cluster growth and aggregation (see Figure 4B).

For HEX-IV (pH = 1.1), from Figures 5A3–C3, we can see that the SRH of HEX-IV falls within the range of 66%–68%. In the period of 0–2,600 s, the reduction in RH leads to an increase in the Raman intensity from the C-H vibrations and a decrease in the intensity from O-H (this phenomenon is more obvious in Figure 5A1). After that, we elevated the ambient RH; the droplet started to absorb the moisture along with a decrease of C-H mode and an increase of O-H mode. Besides, the convoluted WGMs in the spectra regress to around six main peaks at around 3200 s (marked with a grey dashed line in the figure). It means that the droplet subsequently returned to be homogenous, albeit a hysteresis took place compared with the increase of RH. Moreover, the mixing relative humidity (MRH, the RH level at which phase mixing occurs) can be determined according to the slump of the fitting errors, which is in the range of 72%–75% and mildly higher than the SRH. It is inline with the results of Losey et al. [28]. It also shows that water molecules can go through the hydrophobic shell and be absorbed by the hydrophilic core during the process of water condensation. It might stem from that the molecules of organics are much bigger than the molecules of water so that the latter can transfer through the pores and channels formed in the former.

pH dependence of separation relative humidity

The SRHs of aerosol droplets generated from Solution HEX-I ~IV are illustrated in Figure 6. It can be seen that the SRH of HEX decreases as pH decreases, which means that the acid enhances the miscibility of organics/inorganics. Considering the acidity found in ambient aerosol particles, it is conceivable that aerosols would undergo phase separation at lower RH than the values

reported in [17,18]. Moreover, the pH-dependent SRHs reported by Losey et al. [28] are also drawn in the same graph. Our results agree well with that of Losey et al. [28] in the pH range of 3 ~5. The discrepancy occurs when the pH is below 3 and increases in the range of 1 ~2. It may result from the different ambient conditions of the droplets which are laser-levitation (leading to a morphology of sphere) and substrate-deposition (leading to a morphology of spherical crown) respectively. Besides, the researched droplets in our work were also obviously smaller than that in Losey et al. [28]. Considering the realistic size and levitating state, the droplets used in our work better mimicked the natural airborne aerosols Kucinski et al. [40]. found that the size of micro-particles was influential in the phase separation. The smaller size and the spherical morphology enhance the Kelvin effect, making the droplets in our work easier to undergo phase separation.

Conclusion

In this work, we detected the impact of pH on phase separation in multicomponent aerosol droplets, such as OA/NaCl/Water and HEX/$(NH_4)_2SO_4$/Water. To the best of the authors' knowledge, it is the first time to investigate the pH-dependent phase separation at single levitated particle level. The results indicate that pH can change the miscibility of the mixtures, low pH will reduce the SRH of HEX. Besides, pH can also change the phase separated structure, such as pH can change the morphology of OA/NaCl/Water droplet from partially-engulfed to core-shell under certain conditions. Moreover, our results unveil the mass transfer in a core-shell microdroplet that water molecules can go through the hydrophobic shell and be absorbed by the hydrophilic core. This work further informs our understanding of the phase separation of aerosols under real ambient conditions, that the prevalence of phase separation in ambient aerosols perhaps should be reassessed taking account of the acidic environment.

In the future, the phase separation in real acidified ambient aerosols is expected to be further researched, which would provide us with possible implications of the morphology of real aerosols and its impacts on related properties such as the hygroscopicity, homogenous chemistry, and et al.

Data availability statement

The original contributions presented in the study are included in the article/Supplementary Material, further inquiries can be directed to the corresponding author.

Author contributions

Y-KT proposed the idea of the project, performed the measurements, conducted the data analysis, and led in writing the manuscript. AY contributed to funding the research, constructed the optical tweezer system, provided the instruction on the experiment and revised the manuscript. XM discussed the experiment objectives and contents and prepared the aerosol solutions. BZ and RS contributed to the data visualization. ZW was responsible for the conceptualization of aerosol droplets and discussion of methodology.

Funding

This work was supported by the National Natural Science Foundation of China (U19A2007, 32150026 and 92043302) and the National Key Research & Development Program of China (2017YFC0209504).

Acknowledgments

Y-KT gratefully acknowledge Dr Chen Cai for instructive suggestions on experiments.

Conflict of interest

The authors declare that the research was conducted in the absence of any commercial or financial relationships that could be construed as a potential conflict of interest.

Publisher's note

Supplementary material

The Supplementary Material for this article can be found online at: https://www.frontiersin.org/articles/10.3389/fphy.2022.969921/full#supplementary-material

References

1. Du A, Li Y, Sun J, Zhang Z, You B, Li Z, et al. Rapid transition of aerosol optical properties and water-soluble organic aerosols in cold season in fenwei plain. *Sci Total Environ* (2022) 829:154661. doi:10.1016/j.scitotenv.2022.154661

2. Arroyo PC, David G, Alpert PA, Parmentier EA, Ammann M, Signorell R. Amplification of light within aerosol particles accelerates in-particle photochemistry. *Science* (2022) 376:293–6. doi:10.1126/science.abm7915

3. Zhang Y, Chen Y, Lei Z, Olson NE, Riva M, Koss AR, et al. Joint impacts of acidity and viscosity on the formation of secondary organic aerosol from isoprene epoxydiols (iepox) in phase separated particles. *ACS Earth Space Chem* (2019) 3: 2646–58. doi:10.1021/acsearthspacechem.9b00209

4. Lam HK, Xu R, Choczynski J, Davies JF, Ham D, Song M, et al. Effects of liquid–liquid phase separation and relative humidity on the heterogeneous oh oxidation of inorganic–organic aerosols: Insights from methylglutaric acid and ammonium sulfate particles. *Atmos Chem Phys* (2021) 21:2053–66. doi:10.5194/acp-21-2053-2021

5. Pye HOT, Murphy BN, Xu L, Ng NL, Carlton AG, Guo H, et al. On the implications of aerosol liquid water and phase separation for organic aerosol mass. *Atmos Chem Phys* (2017) 17:343–69. doi:10.5194/acp-17-343-2017

6. Li W, Teng X, Chen X, Liu L, Xu L, Zhang J, et al. Organic coating reduces hygroscopic growth of phase-separated aerosol particles *Environ Sci Technol* (2021) 55:16339–46. doi:10.1021/acs.est.1c05901

7. Petters MD, Kreidenweis SM. A single parameter representation of hygroscopic growth and cloud condensation nucleus activity. *Atmos Chem Phys* (2007) 7: 1961–71. doi:10.5194/acp-7-1961-2007

8. Altaf MB, Dutcher DD, Raymond TM, Freedman MA. Effect of particle morphology on cloud condensation nuclei activity. *ACS Earth Space Chem* (2018) 2: 634–9. doi:10.1021/acsearthspacechem.7b00146

9. Freedman MA. Liquid–liquid phase separation in supermicrometer and submicrometer aerosol particles. *Acc Chem Res* (2020) 53:1102–10. doi:10.1021/acs.accounts.0c00093

10. Mikhailov EF, Pöhlker ML, Reinmuth-Selzle K, Vlasenko SS, Krüger OO, Fröhlich-Nowoisky J, et al. Water uptake of subpollen aerosol particles: Hygroscopic growth, cloud condensation nuclei activation, and liquid–liquid phase separation. *Atmos Chem Phys* (2021) 21:6999–7022. doi:10.5194/acp-21-6999-2021

11. You Y, Smith ML, Song M, Martin ST, Bertram AK. Liquid–liquid phase separation in atmospherically relevant particles consisting of organic species and inorganic salts. *Int Rev Phys Chem* (2014) 33:43–77. doi:10.1080/0144235X.2014.890786

12. Freedman MA. Phase separation in organic aerosol. *Chem Soc Rev* (2017) 46: 7694–705. doi:10.1039/C6CS00783J

13. Kwamena N-OA, Buajarern J, Reid JP. Equilibrium morphology of mixed organic/inorganic/aqueous aerosol droplets: Investigating the effect of relative humidity and surfactants. *J Phys Chem A* (2010) 114:5787–95. doi:10.1021/jp1003648

14. Reid JP, Dennis-Smither BJ, Kwamena N-OA, Miles REH, Hanford KL, Homer CJ. The morphology of aerosol particles consisting of hydrophobic and hydrophilic phases: Hydrocarbons, alcohols and fatty acids as the hydrophobic component. *Phys Chem Chem Phys* (2011) 13:15559–72. doi:10.1039/C1CP21510H

15. Stewart DJ, Cai C, Nayler J, Preston TC, Reid JP, Krieger UK, et al. Liquid–liquid phase separation in mixed organic/inorganic single aqueous aerosol droplets *J Phys Chem A* (2015) 119:4177–90. doi:10.1021/acs.jpca.5b01658

16. Ishizaka S, Yamamoto C, Yamagishi H. Liquid–liquid phase separation of single optically levitated water–ionic liquid droplets in air. *J Phys Chem A* (2021) 125:7716–22. doi:10.1021/acs.jpca.1c06130

17. Pöhlker C, Wiedemann KT, Sinha B, Shiraiwa M, Gunthe SS, Smith M, et al. Biogenic potassium salt particles as seeds for secondary organic aerosol in the amazon. *Science* (2012) 337:1075–8. doi:10.1126/science.1223264

18. You Y, Renbaum-Wolff L, Carreras-Sospedra M, Hanna SJ, Hiranuma N, Kamal S, et al. Images reveal that atmospheric particles can undergo liquid–liquid phase separations. *Proc Natl Acad Sci U S A* (2012) 109:13188–93. doi:10.1073/pnas.1206414109

19. Lee HD, Morris HS, Laskina O, Sultana CM, Lee C, Jayarathne T, et al. Organic enrichment, physical phase state, and surface tension depression of nascent core–shell sea spray aerosols during two phytoplankton blooms. *ACS Earth Space Chem* (2020) 4:650–60. doi:10.1021/acsearthspacechem.0c00032

20. Weber RJ, Guo H, Russell AG, Nenes A. High aerosol acidity despite declining atmospheric sulfate concentrations over the past 15 years. *Nat Geosci* (2016) 9: 282–5. doi:10.1038/ngeo2665

21. Song S, Gao M, Xu W, Shao J, Shi G, Wang S, et al. Fine-particle ph for beijing winter haze as inferred from different thermodynamic equilibrium models. *Atmos Chem Phys* (2018) 18:7423–38. doi:10.5194/acp-18-7423-2018

22. Liu M, Huang X, Song Y, Tang J, Cao J, Zhang X, et al. Ammonia emission control in China would mitigate haze pollution and nitrogen deposition, but worsen acid rain. *Proc Natl Acad Sci U S A* (2019) 116:7760–5. doi:10.1073/pnas.1814880116

23. Jia S, Chen W, Zhang Q, Krishnan P, Mao J, Zhong B, et al. A quantitative analysis of the driving factors affecting seasonal variation of aerosol ph in guangzhou, China. *Sci Total Environ* (2020) 725:138228. doi:10.1016/j.scitotenv.2020.138228

24. Angle KJ, Crocker DR, Simpson RMC, Mayer KJ, Garofalo LA, Moore AN, et al. Acidity across the interface from the ocean surface to sea spray aerosol. *Proc Natl Acad Sci U S A* (2021) 118:e2018397118. doi:10.1073/pnas.2018397118

25. Zhang B, Shen H, Liu P, Guo H, Hu Y, Chen Y, et al. Significant contrasts in aerosol acidity between China and the United States. *Atmos Chem Phys* (2021) 21: 8341–56. doi:10.5194/acp-21-8341-2021

26. Dallemagne MA, Huang XY, Eddingsaas NC. Variation in ph of model secondary organic aerosol during liquid–liquid phase separation. *J Phys Chem A* (2016) 120:2868–76. doi:10.1021/acs.jpca.6b00275

27. Losey DJ, Parker RG, Freedman MA. Ph dependence of liquid–liquid phase separation in organic aerosol. *J Phys Chem Lett* (2016) 7:3861–5. doi:10.1021/acs.jpclett.6b01621

28. Losey DJ, Ott E-JE, Freedman MA. Effects of high acidity on phase transitions of an organic aerosol. *J Phys Chem A* (2018) 122:3819–28. doi:10.1021/acs.jpca.8b00399

29. Zhou Q, Pang S-F, Wang Y, Ma J-B, Zhang Y-H. Confocal Raman studies of the evolution of the physical state of mixed phthalic acid/ammonium sulfate aerosol droplets and the effect of substrates. *J Phys Chem B* (2014) 118:6198–205. doi:10.1021/jp5004598

30. Tong Y, Fang T, Liu Y, Zhao D, Ye A. Research on hygroscopicity and volatility of single aerosol droplet. *J Atmos Environ Opt* (2020) 15:486–95. doi:10.3969/j.issn.1673-6141.2020.06.008

31. Tong Y-K, Liu Y, Meng X, Wang J, Zhao D, Wu Z, et al. The relative humidity-dependent viscosity of single quasi aerosol particles and possible implications for atmospheric aerosol chemistry. *Phys Chem Chem Phys* (2022) 24:10514–23. doi:10.1039/D2CP00740A

32. Ma S, Chen Z, Pang S, Zhang Y. Observations on hygroscopic growth and phase transitions of mixed 1, 2, 6-hexanetriol/(NH₄)₂SO₄ particles: Investigation of the liquid–liquid phase separation (LLPS) dynamic process and mechanism and secondary LLPS during the dehumidificationso$_4$ particles: Investigation of the liquid–liquid phase separation (llps) dynamic process and mechanism and secondary llps during the dehumidification. *Atmos Chem Phys* (2021) 21:9705–17. doi:10.5194/acp-21-9705-2021 $(nh_4)_2$

33. Gorkowski K, Beydoun H, Aboff M, Walker JS, Reid JP, Sullivan RC. Advanced aerosol optical tweezers chamber design to facilitate phase-separation and equilibration timescale experiments on complex droplets. *Aerosol Sci Technology* (2016) 50:1327–41. doi:10.1080/02786826.2016.1224317

34. Gorkowski K, Donahue NM, Sullivan RC. Emerging investigator series: Determination of biphasic core–shell droplet properties using aerosol optical tweezers. *Environ Sci : Process. Impacts* (2018) 20:1512–23. doi:10.1039/C8EM00166A

35. Gorkowski K, Donahue NM, Sullivan RC. Aerosol optical tweezers constrain the morphology evolution of liquid-liquid phase-separated atmospheric particles. *Chem* (2020) 6:204–20. doi:10.1016/j.chempr.2019.10.018

36. Sullivan RC, Boyer-Chelmo H, Gorkowski K, Beydoun H. Aerosol optical tweezers elucidate the chemistry, acidity, phase separations, and morphology of atmospheric microdroplets. *Acc Chem Res* (2020) 53:2498–509. doi:10.1021/acs.accounts.0c00407

37. Preston TC, Reid JP. Determining the size and refractive index of microspheres using the mode assignments from mie resonances. *J Opt Soc Am A* (2015) 32:2210–7. doi:10.1364/JOSAA.32.002210

38. Mellouki A, Wallington TJ, Chen J. Atmospheric chemistry of oxygenated volatile organic compounds: Impacts on air quality and climate. *Chem Rev* (2015) 115:3984–4014. doi:10.1021/cr500549n

39. Zhang Y, Chen Y, Lambe AT, Olson NE, Lei Z, Craig RL, et al. Effect of the aerosol-phase state on secondary organic aerosol formation from the reactive uptake of isoprene-derived epoxydiols (iepox). *Environ Sci Technol Lett* (2018) 5:167–74. doi:10.1021/acs.estlett.8b00044

40. Kucinski TM, Dawson JN, Freedman MA. Size-dependent liquid–liquid phase separation in atmospherically relevant complex systems. *J Phys Chem Lett* (2019) 10:6915–20. doi:10.1021/acs.jpclett.9b02532